Nanoscale

PAPER

Cite this: *Nanoscale*, 2015, **7**, 2433

Laser beam controlled drug release from Ce6–gold nanorod composites in living cells: a FLIM study

Yongkui Xu,* Ruoyu He, Dongdong Lin, Minbiao Ji* and Jiyao Chen

Received 23rd September 2014,
Accepted 19th December 2014

DOI: 10.1039/c4nr05574h

www.rsc.org/nanoscale

A new method to image drug release from drug–nanoparticle composites in living cells was established. The composites of silica coated gold nanorods (AuNR@SiO_2) and chlorine e6 (Ce6) photosensitizers (AuNR@SiO_2–Ce6) were formed by electrostatic force with a Ce6 loading efficiency of 80%. The strong resonance absorptions of AuNR@SiO_2–Ce6 in the near-infrared (NIR) region enabled the effective release of Ce6 from AuNR@SiO_2–Ce6 by 780 nm CW laser irradiation. The 780 nm laser beam was applied to not only control the releasing amount of Ce6 from cellular AuNR@SiO_2–Ce6 by adjusting the irradiation dose (time), but also to spatially confine the Ce6 release in cells by focusing the laser beam on the target sites. Furthermore, the fluorescence lifetime of Ce6 was found to change drastically from 0.9 ns in the AuNR@SiO_2–Ce6 complex to 6 ns after release, and therefore fluorescence lifetime imaging microscopy (FLIM) was introduced to image the photo-induced Ce6 release in living cells. Finally, the controllable killing effect of photodynamic cancer therapy (PDT) using AuNR@SiO_2–Ce6 was demonstrated by changing the released amount of Ce6, which indicates that AuNR@SiO_2–Ce6 is promising for targeted tumour PDT.

1. Introduction

With the rapid development of nanotechnology, nanoparticles have been suggested as the carriers for efficient drug delivery because of their versatile physical and chemical properties.[1–4] Some nanovehicles such as mesoporous silica nanoparticles are able to load a great amount of drugs and release them in living systems by slow diffusion.[1,5,6] However, for these nanoparticles, a controlled release in targeted sites of the living body is difficult to achieve and better strategies are needed.[7] Gold nanoparticles have been widely used in biomedicine research[8] such as metal enhanced fluorescence[9–12] and photothermal therapy,[13,14] due to their chemical inertness, minimum biological toxicity and strong light absorption resulting from surface plasmon resonance (SPR).[15] Gold nanocubes can bring two orders of magnitude fluorescence enhancement of aluminium phthalocyanine.[15] Gold nanorods (AuNRs) can be used in the photo-thermal therapy of cancers and can even be used as nanobombs to destroy cancer cells under the irradiation of NIR femtosecond (fs) laser.[16] With suitable aspect ratios of about 4–5, AuNRs have strong absorption in the NIR region, which is the so-called tissue optical window, because of superior light penetration. Importantly, the photothermal effect of AuNRs allows controllable drug release from the AuNR–drug composites through the spatial and temporal management of NIR light irradiation.[17–19] The idea of using AuNRs to release drugs by light sounds reasonable. However, the quantitative measurement of drugs released from the AuNR–drug is a great challenge. If the releasing measurement is not established, the potential of this modality for controlled drug release cannot be evaluated. In this work, we have established a method for imaging drug release in living cells by fluorescence lifetime imaging microscope (FLIM) based on the fact that the fluorescence lifetime of certain drugs varies remarkably along different positions with respect to the AuNRs.[20] Herein a well-known photosensitizer for the photodynamic therapy (PDT) of cancers, chlorin e6 (Ce6), was applied as the fluorescent drug. Our results confirmed that FLIM is a powerful tool to study the releasing process of Ce6 from AuNR@SiO_2–Ce6 composites in living cells by controlling the irradiation dose of a 780 nm laser. Furthermore, *in vitro* PDT experiments showed that the PDT effect of the AuNR@SiO_2–Ce6 composites can be administrated by controlling the amount of Ce6 released. The controllable PDT effect would be very useful in PDT practice by photo-releasing photosensitizers from composite carriers at the tumour site only thus preventing skin photo-toxicity.

State Key Laboratory of Surface Physics and Department of Physics, and Key Laboratory of Micro and Nano Photonic Structures (Ministry of Education), Fudan University, 220 Handan road, Yanpu District, Shanghai 200433, China. E-mail: 12110190045@fudan.edu.cn, minbiaoj@fudan.edu.cn

2. Results and discussion

CTAB-stabilized gold nanorods, amino group modified mesoporous silica shell coated gold nanorods (AuNR@SiO_2) and amino group modified mesoporous silica nanoparticles (MSNs) were prepared. The characterization of the as-prepared nanoparticles was undertaken. TEM images of AuNRs, AuNR@SiO_2 and MSNs are shown in Fig. 1(A–C). The sizes of the particles synthesized were about 50 nm. The optimal goal of targeted drug delivery is to deliver active drugs to specific tumour sites while minimizing the side effects of the drugs on normal tissues. One way to do this is *via* active tumour targeting through receptor-mediated endocytosis by modifying the surface of nanoparticles with ligands.[21] However, such an approach has been questioned for drawbacks that limit its efficacy, such as decreased blood circulation time and reduced tumour penetration.[22] In this work, we chose to use the passive targeting approach. Due to the enhanced permeability and retention (EPR) effect of tumour tissues, nanoparticles could selectively penetrate through the defective tumour vasculatures accumulating in tumours, achieving targeted deliveries.[23] So instead of modifying the surface of nanoparticles with ligands, we modified it with amino groups, making it positively charged for easier cell endocytosis. AuNRs have two SPR bands with the transverse surface plasmon resonance (TSPR) band at 530 nm and the longitudinal surface plasmon resonance (LSPR) band around 760 nm, corresponding to the aspect ratio of 3.7, according to the absorption spectrum showed in Fig. 1(D). Compared to the absorption spectrum of AuNRs, AuNR@SiO_2 shows an enhanced absorption at TSPR and a red shift band of LSPR at 780 nm. The MSNs absorb some visible light and appear milky.

In this work, we used a soluble form of the Ce6 derivative – sodium iron chlorophyllin, which was still called Ce6 for convenience. The molecular structure is shown in Fig. 1E. The absorption and fluorescence spectra are also exhibited in Fig. 1E. Ce6 has two absorption bands located around 405 nm (B band) and 660 nm (Q band), and its fluorescence band is at 660 nm. Since each Ce6 molecule possesses 3 negatively charged side carboxylic groups, it is easy to bind on the surface of positively charged nanoparticles to form conjugates. Although the CTAB stabilized AuNRs can well disperse in an aqueous solution and conjugate with Ce6, the toxicity of CTAB is a great concern. Therefore, we coated the AuNRs with biocompatible silica shells making AuNR@SiO_2 less toxic with an increased drug loading ability.

The Ce6 loading experiment was carried out subsequently. The loading ability of each kind of nanoparticle can be measured by the fluorescence comparison of Ce6 before and after loading. After mixing 5 μL of 1 mM Ce6 with 0.3 mL of 100 pM AuNR, AuNR@SiO_2 or MSN, and shaking overnight, the composites AuNR–Ce6, AuNR@SiO_2–Ce6 and MSN–Ce6 were formed, respectively. These composite samples were centrifuged to separate the composites at the bottom of the centrifuge tube and the unloaded free Ce6 in the supernatant. By comparing the fluorescence intensity of the unloaded Ce6 in the supernatant for each case with that of Ce6 at the original concentration (5 μM) before the conjugation, the Ce6 loading ratio for each case can be evaluated. As shown in Fig. 2A, the loading ratios were obviously different for these composites which can be seen from the fluorescence spectra/intensities

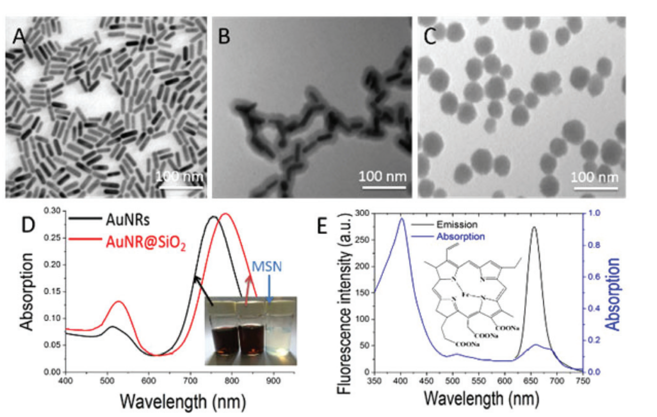

Fig. 1 Characterization of AuNRs, AuNR@SiO_2 and MSNs. (A), (B) and (C) are their corresponding TEM images. (D) Shows the absorption spectra of AuNRs and AuNR@SiO_2 and pictures of AuNRs, AuNR@SiO_2 and MSNs in aqueous solutions. (E) Shows the molecular structure of Ce6 and the absorption and fluorescence spectra of Ce6 with a concentration of 5 μM under an excitation of 405 nm.

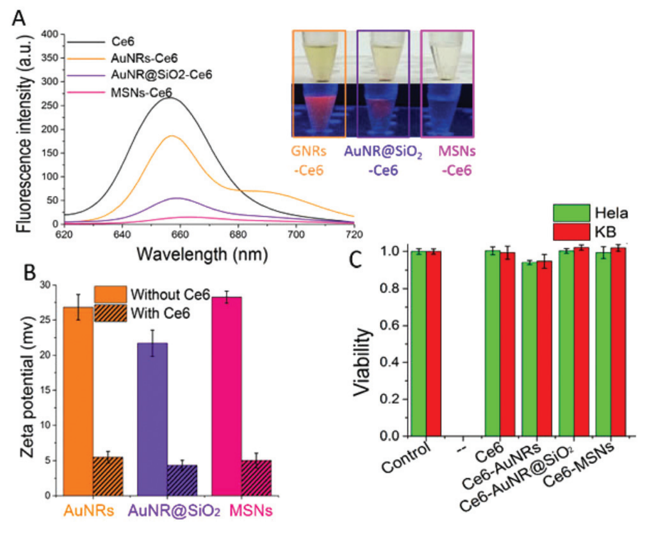

Fig. 2 (A) Comparison of the Ce6 loading of three kinds of nanoparticles by measuring the fluorescence of the un-conjugated Ce6 left in the supernatant fluid of each composite after centrifugation. The upper row of insert shows the common photos of these samples and the lower row of the insert gives the fluorescence photographs of the supernatants of these samples under the irradiation of a UV beam of 365 nm. (B) Zeta potentials of AuNRs, AuNR@SiO_2, MSNs before and after Ce6 conjugation. (C) Cytotoxicities of the used compounds on Hela and KB cells. The incubation concentration of Ce6 was 5 μM and those of the composites of Ce6 to nanoparticles were 5 μM to 30 pM and the incubation time was 2 hours. The control groups were cells without any treatment.

comparison and visual observation under UV excitation. The loading ratio can be calculated according to the following formula (1)

$$\text{loading ratio} = 1 - \frac{\text{fluorescence intensity of supernatant}}{\text{fluorescence intensity of } 5\,\mu\text{M Ce6}} \tag{1}$$

For the MSN–Ce6 composites, the loading ratio reached 95% demonstrating that the MSNs were good drug carriers. The loading ratio of $AuNR@SiO_2$–Ce6 was 80%, much higher than that of AuNR–Ce6 (34%), indicating that $AuNR@SiO_2$–Ce6 was also a suitable composite for Ce6 loading.

Since these three kinds of nanoparticles were all positively charged, their zeta potentials were in the region of +20 to +30 mV. When Ce6 molecules (5 μM) were linked to these nanoparticles, the zeta potentials of all the composites decreased to about +5 mV (Fig. 2B), indicating that conjugation was established. The cytotoxicities of these composites were measured using Hela and KB cell lines as *in vitro* models. As shown in Fig. 2C, after 2 hours of incubation an observable toxicity was seen for the AuNR–Ce6 composites which induced 10% cell damage. Such toxicity of AuNR–Ce6 is reasonable as the surface CTAB of AuNRs was a known toxic agent. The toxicity of $AuNR@SiO_2$–Ce6 was reduced as almost no significant damage could be found. The silicon shell is much safer than CTAB, so $AuNR@SiO_2$–Ce6 was selected for the next-step drug releasing experiments.

Since the LSPR band of AuNRs is located at 780 nm, irradiation by a 780 nm laser may produce a photo-thermal effect on AuNRs thus increasing their temperature, resulting in the release of Ce6 from $AuNR@SiO_2$–Ce6. The middle power of a 100 mW 780 nm laser was used to irradiate the composite aqueous solutions. After a certain dose of irradiation, the composite solution was centrifuged to separate the supernatant and the $AuNR@SiO_2$–Ce6 composite at the bottom of the centrifuge tube, and then the supernatant was collected for fluorescence intensity measurements to determine the amount of Ce6 released in the supernatant. The release of the two composites, $AuNR@SiO_2$–Ce6 and MSN–Ce6, in an aqueous solution was studied. As shown in Fig. 3A, no obvious release of Ce6 could be found for MSN–Ce6 after 780 nm laser irradiations, because MSNs have little absorption at 780 nm and thus the photothermal effect can be neglected. Therefore, MSNs are not good candidates for a light controlled drug release study. With an increased irradiation dose of the 780 nm laser, the Ce6 release from $AuNR@SiO_2$–Ce6 was enhanced accordingly and a remarkable release (80%) of Ce6 molecules was achieved after 2 J dose irradiation of the 780 nm laser, indicating that $AuNR@SiO_2$ composites are suitable carriers for light controlled drug release. Such releasing courses are sketched in Fig. 3B. This result confidently demonstrates that the 780 nm laser can conveniently control the Ce6 release from $AuNR@SiO_2$–Ce6 in an aqueous solution. However, the interesting point for monitoring drug release is how to measure such a controlled release in living systems. The above mentioned fluorescence intensity measurement in a supernatant after irradiation is certainly not suitable for living systems and other detection ways to measure the controlled release need to be established. Based on the theory of metal-enhanced fluorescence (MEF), the SPR in metal particles brings a new radiative rate Γ_m to the attached fluorophores, and thus the lifetime τ of the fluorophores is shortened as described with the radiative rate Γ and the non-radiative rate k_{nr} in the following formula:[24]

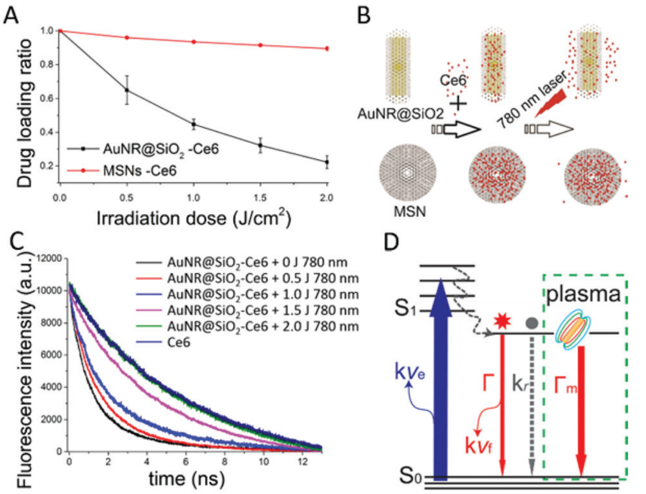

Fig. 3 (A) Comparison of Ce6 releases from $AuNR@SiO_2$–Ce6 and MSN–Ce6 in aqueous solutions under the irradiation of a 780 nm laser. (B) The sketch map of Ce6 loading and release by $AuNR@SiO_2$ and MSNs. (C) Fluorescence lifetime changes of $AuNR@SiO_2$–Ce6 aqueous solution under the irradiation of a 780 nm laser with different doses. (D) Energy level diagram and schematic representation of energy transfer path involved in AuNR-enhanced Ce6.

$$\tau = 1/(\Gamma_m + \Gamma + k_{nr}) \tag{2}$$

The fluorescence lifetimes of free Ce6 and conjugated Ce6 in $AuNR@SiO_2$–Ce6 in an aqueous solution were measured firstly to confirm the lifetime difference between the two cases. As shown in Fig. 3C, the fluorescence lifetime of unconjugated Ce6 is 6.29 ns, whereas that of conjugated Ce6 is greatly shortened to 0.91 ns. Therefore the fluorescence lifetime difference can be used to measure Ce6 release from $AuNR@SiO_2$–Ce6 composites. As shown in Fig. 3A, under the irradiation of a 780 nm laser the conjugated Ce6 is gradually released from $AuNR@SiO_2$–Ce6. In these situations, the solutions contained the released free Ce6 and conjugated Ce6 in $AuNR@SiO_2$–Ce6 so that the fluorescence lifetime of the solution should be the average of the two components according to their corresponding percentages. With an increased irradiation dose of the 780 nm laser, the fluorescence lifetime gradually approached that of free Ce6. With an irradiation dose of 2 J, the fluorescence lifetime curve almost overlapped with that of free Ce6 totally (Fig. 3C), because in this situation most Ce6 molecules had been released into the solution. Based on these results, the fluorescence lifetime change can

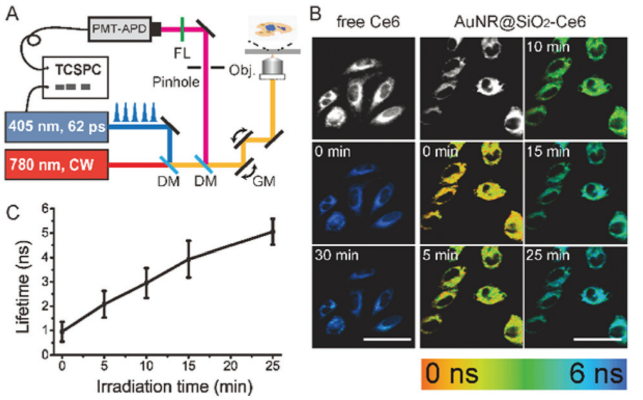

Fig. 4 (A) Setup schematics of the fluorescence lifetime and FLIM experiments. (B) Fluorescence images of KB cells incubated with free Ce6 (first column) and AuNR@SiO_2–Ce6 (second and third columns). Fluorescence intensity images are shown in gray, and FLIM images of these cells under different irradiation times of 2 mW 780 nm laser are shown in false-colour with the colour map indicating the fluorescence lifetime. (C) The time-dependent mean fluorescence lifetime of all pixels in the fluorescence lifetime images of the AuNR@SiO_2–Ce6 incubated KB cells after irradiation. DM: dichroic mirror, GM: galvo mirror, FL: filter. Scale bar: 100 μm.

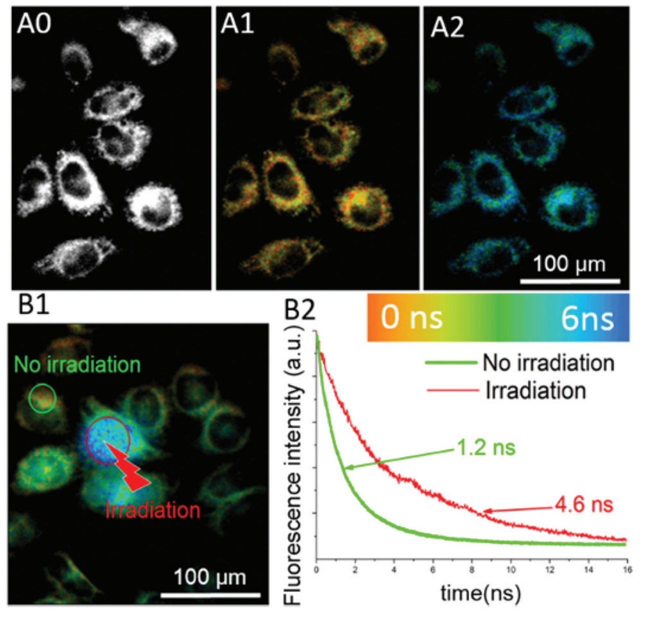

Fig. 5 (A) The fluorescence intensity image of AuNR@SiO_2–Ce6 incubated Hela cells (A0) and the corresponding fluorescence lifetime images of cells before (A1) and after (A2) irradiation of 2 mW with a 780 nm laser for 30 minutes with a repetitive *x*–*y* scanning mode. (B) The fluorescence lifetime images of AuNR@SiO_2–Ce6 incubated cells after irradiation of 2 mW with a 780 nm laser for 3 minutes with a point-scan mode. (B1) In B1, a red circle marked a part of the cell which had been irradiated by a 780 nm laser before the FLIM image was acquired. (B2) Shows the fluorescence lifetime decay curves of the 780 nm laser irradiated area and the un-irradiated area (green circled areas) in (B1).

be used as a sensitive tool to further measure the Ce6 releasing from AuNR@SiO_2–Ce6 in the living cells *in situ*.

Our experimental setup is shown in Fig. 4A. A 780 nm CW laser was introduced into the microscope as the controlling light for Ce6 release from cellular AuNR@SiO_2–Ce6; another 405 nm picosecond (ps) pulsed laser was used for fluorescence excitation. By measuring the time elapsed between the excitation laser pulses and fluorescence photons with time-correlated single-photon counting (TCSPC), we can calculate the lifetime of the excited fluorophores at each laser focus. A fluorescence lifetime imaging microscope (FLIM) therefore maps the fluorescence lifetimes pixel by pixel as the laser scans through the sample using a pair of galvo mirrors. FLIM is practicable for imaging fluorescence lifetime changes during relatively slow (normally >30 s) dynamic processes in a small area giving the quasi real time mapping of fluorescence lifetime in a living cell.[25] After incubation with free Ce6 (5 μM) or AuNR@SiO_2–Ce6 (20 pM–5 μM) the drug loaded KB cells were measured with FLIM, while a 2 mW 780 nm laser was used to photo-release Ce6 from AuNR@SiO_2–Ce6 (Fig. 4B). As a control, the fluorescence lifetimes of Ce6 in the free Ce6 treated KB cells were maintained around 6 ns before and after 30 min of 780 nm irradiation. In contrast, the fluorescence lifetimes of Ce6 in the AuNR@SiO_2–Ce6 incubated KB cells changed gradually from 0.9 ns to 5 ns as the irradiation time of the 780 nm laser increased to 25 min. Such changes could be clearly seen in the false-coloured FLIM images shown in Fig. 4B, indicating that Ce6 molecules were released from cellular AuNR@SiO_2–Ce6 composites under 780 nm laser irradiation. Fig. 4C shows the statistical change of Ce6 lifetimes of the AuNR@SiO_2–Ce6 composite incubated cells under irradiation for different times. These results demonstrated for the first time that FLIM could serve as a powerful tool to measure the dynamic fluorescence drug release from plasma particles *in vitro*.

Fig. 5A shows the FLIM images of Ce6–AuNR@SiO_2 in another cell line (Hela cells) before and after irradiation with the 780 nm laser for 30 min. Statistically, from Fig. 5A1 to A2, the average fluorescence lifetime was about 1 ns before irradiation and turned out to be 4.6 ns after irradiation with the 2 mW 780 nm laser for 30 minutes, confirming the release of Ce6 from AuNR@SiO_2–Ce6 conjugates. To further demonstrate the precise control of Ce6 release in cells by the 780 nm laser, we used the point-scan model (without scanning) to irradiate a select small area on a cell with the 780 nm laser for 3 min leaving the other area un-irradiated, and then the FLIM images of these cells were acquired as shown in Fig. 5B1. The blue colour (with a lifetime of about 5 ns) of the 780 nm laser irradiated area obviously differs from the yellow-green colour (with a lifetime of around 1 ns) of the un-irradiated regions. Fig. 5B2 gives the fluorescence lifetimes of the 780 nm irradiated area and the un-irradiated region as circled in Fig. 5B1, and the corresponding lifetimes of 4.6 ns and 1.2 ns, respectively, support that the 780 nm laser beam can control Ce6 release in the micro-region of the living cell. When a 2 mW light is tight-focused into a micrometre area (power density ~200 kW cm^{-2}) with continuous irradiation the damage becomes obvious, as can be seen from Fig. 5B1 where the nucleus of the cell chosen to be irradiated was destroyed. Due to the fact that the absorption efficiency of AuNRs depends greatly on their distribution and arrangement, there is no accurate temperature rise calculation method with irradiation. Here we estimate the temperature of AuNRs in a water solution under continuous 780 nm irradiation by the following calculation using the steady state thermal diffusion equation:

$$P_{\mathrm{I}}\sigma_{\mathrm{AuNRs}} = G_{\mathrm{Au\text{-}water}}S_{\mathrm{AuNR}}(T_{\mathrm{AuNR}} - T_{\mathrm{water}}) \tag{3}$$

where T_{AuNR} and T_{water} are the temperatures of AuNRs and the surrounding water, respectively, set as 300 K considering the high heat capacity of water and the high volume ratio of water to AuNRs. The laser energy absorbed by AuNRs depends on the laser fluence P_{I}, and the absorption cross-sectional area σ_{AuNR}. $G_{\mathrm{Au\text{-}water}}$ is the thermal conductance at the AuNR–water interface. S_{AuNR} is the surface area of the AuNRs. And according to the system parameters and properties of the nanoparticles, we can get an approximate temperature of 1100 K for AuNRs which is high enough to scald the cell apparatus. But with the *x*–*y* repeat scan model, there is only 4.3 μs 780 nm irradiation for every pixel in each circle. Considering that the heat diffusion to the water solution in the laser focus together with the concentration of AuNRs is supposed to be 1 μM, the temperature of the surroundings rises less than 1 K, making little thermal damage on the cells.

To cure a localized disease, specifically targeted drug delivery is the goal of medical researchers. However, so far the targeting effect of drugs is still limited due to the complexity of the living systems. Generally, when drugs are delivered into a living body, they reach both the diseased site and the normal tissues inducing the therapy effect and causing side-effects on normal tissues probably. Controlled drug delivery is a promising strategy for drug delivery which uses a carrier to load drugs and releases the drugs from the carrier only at the diseased site in a controlled manner. Controlled drug delivery can certainly decrease side-effects and improve the therapeutic effect by efficient and thorough drug-release, but it is challenged by the use of a controlled manner which should be feasible and practicable. In this work, we found that AuNR@SiO_2 is a suitable carrier and the NIR laser beam irradiation is a good way to release drugs from the AuNR@SiO_2–drug composites due to the strong absorptions at the LSPR band. With AuNR@SiO_2–Ce6, an effective light controlled Ce6 release was achieved *in vitro* here.

The purpose of controlled drug release is to release drugs at the desired site for therapy. The ability of AuNR@SiO_2–Ce6 to release Ce6 for therapy was then checked. Ce6, a photosensitizer, is known as an efficient $^1O_2$ producer. The PDT effects of Ce6 and AuNR@SiO_2–Ce6 depend on their $^1O_2$ production. $^1O_2$ is a short-distance reactive agent because of its short lifetime. So, in this work, AuNR@SiO_2–Ce6 was designed as a poor $^1O_2$ producer, and the photo-released Ce6 from AuNR@SiO_2–Ce6 was a good $^1O_2$ generator. Using DBPF as a sensitive $^1O_2$ probe, the $^1O_2$ production of AuNR@SiO_2–Ce6 in an aqueous solution was measured when the sample solution had been irradiated by a 650 nm light beam which is at the absorption

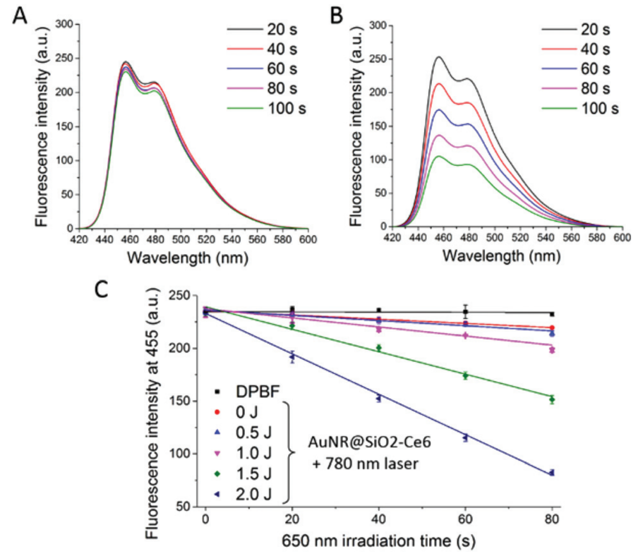

Fig. 6 The fluorescence intensity change of DPBF at 455 nm with the irradiation times (0–100 s) of 650 nm CW light beam (10 mW). (A) For the AuNR@SiO_2–Ce6 aqueous solution without pre-irradiation with a 780 nm laser. (B) For the AuNR@SiO_2–Ce6 sample which has been pre-irradiated by a 780 nm laser with a light dose of 2 J. (C) The DBPF degradations for AuNR@SiO_2–Ce6 samples which have been pre-irradiated by a 780 nm laser with different doses. The excitation for DPBF fluorescence was 405 nm.

Q band of Ce6. Fig. 6A shows that the $^1O_2$ production of AuNR@SiO_2–Ce6 aqueous solution (without pre-irradiation with a 780 nm laser) under the irradiation of a 650 nm light beam is relatively low as expected. When Ce6 was captured in the mesoporous silica shell of AuNR@SiO_2, the excited Ce6 had less chances of colliding with O_2 to produce $^1O_2$ because only a small amount of O_2 diffused into the mesoporous silica shell. Moreover, even if $^1O_2$ was produced in the mesoporous silica shell, such $^1O_2$ would disappear before it encountered and oxidized DBPF, and for this reason only a small amount of DBPF existed in the mesoporous silica shell. When Ce6 is photo-released from AuNR@SiO_2–Ce6 by pre-irradiation with a 780 nm laser, the $^1O_2$ production should increase. For the sample solution of AuNR@SiO_2–Ce6 which has been pre-irradiated by a 780 nm laser with an irradiation dose of 2 J to release most of the attached Ce6, the $^1O_2$ production is so obvious that DBPF is rapidly degraded with the irradiation of a 650 nm light (Fig. 6B). For the sample solution of AuNR@SiO_2–Ce6 which has been pre-irradiated by a 780 nm laser with an irradiation dose less than 2 J, the DBPF degradation rate is relatively lower than that in Fig. 6B and summarized in Fig. 6C. Therefore, the photosensitization ability of AuNR@SiO_2–Ce6 can be modified by controlling the Ce6 release from AuNR@SiO_2–Ce6 with the pre-irradiation of a 780 nm laser beam. The controllable photosensitization ability of AuNR@SiO_2–Ce6 would be very useful in PDT applications as we can only release Ce6 from AuNR@SiO_2–Ce6 at the tumour site by irradiation with a 780 nm laser beam and thus decrease the photo-toxicity in normal tissues.

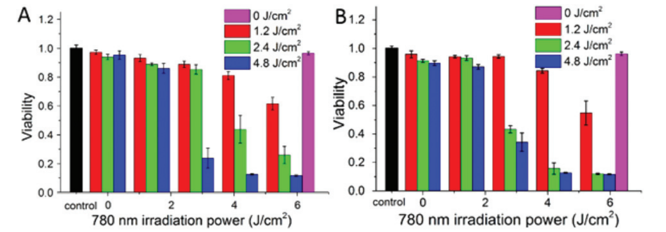

Fig. 7 The relationship of cell viability without (the control group shown as the black bars) and with the pre-irradiation dose of a 780 nm laser. Cells have been incubated with AuNR@SiO_2–Ce6 and irradiated by a 650 nm light (10 mW cm^{-2}) to carry out PDT. (A) KB cells; (B) Hela cells. The incubation concentration of AuNR@SiO_2–Ce6 was 20 pM–5 μM. The values of a 780 nm irradiation dose are 0, 1.4, 2.8, 4.2 and 5.6 J cm^{-2}.

The controllable photosensitization ability of AuNR@SiO_2–Ce6 was subsequently studied *in vitro*. Cells were incubated with AuNR@SiO_2–Ce6 (20 pM–5 μM) for 3 h. Before the 650 nm light irradiation for PDT killing, these composite loaded cell samples in the wells of a 96 well culture plate were pre-irradiated with different doses of a 250 mW cm^{-2} 780 nm laser. Then after the 650 nm light irradiation, cell samples were measured by the MTT assay. Fig. 7A and B show the corresponding PDT results on KB and Hela cells. When the composite loaded cells were not pre-irradiated with a 780 nm laser, PDT damaging was negligible. It can be understood that the bound Ce6 in AuNR@SiO_2–Ce6 is a poor $^1O_2$ generator as shown in Fig. 6. For the cell samples which have been pre-irradiated with a 780 nm laser, the PDT effect occurred and its killing efficiency was proportional to the irradiation dose of 780 nm pre-irradiation. The consistent PDT results on both KB and Hela cells confirmed that the 780 nm light could govern the PDT effect of AuNR@SiO_2–Ce6 by controlling the Ce6 release. In addition, according to the purple columns, when cell samples were pre-irradiated by the 780 nm laser with the high dose of 5.6 J cm^{-2} but not irradiated with the 650 light beam, the damaging effects on these cells were very slight compared with the control group. This result indicates that a 780 nm laser irradiation with a power density of 250 mW cm^{-2} can photo-release Ce6 from cellular AuNR@SiO_2–Ce6 but not directly damage the cells. 780 nm is an NIR wavelength in the optical window region of a living body. The NIR lights were found to be safe for living systems. Therefore using NIR light to control drug release from metal nanoparticles could be a promising way for controlled drug release.

3. Experimental section

3.1. Materials

$HAuCl_4$, hexadecyltrimethylammonium bromide (CTAB), $NaBH_4$, $AgNO_3$, L-ascorbic, (3-aminopropyl)triethoxysilane (APTES), tetraethyl orthosilicate (TEOS) and ethyl acetate (EtoAc) were obtained from Sigma-Aldrich. Ce6 was obtained from Frontier Scientific, Logan, UT, USA. NaOH was obtained from Aladdin Industrial Inc. The D.I. water was self-produced with ion resins. 3-Diphenylisobenzofuran (DPBF) was obtained from J&K Chemical.

Hela cells (human epithelial cervical cancer cell line) and KB cells (a sub-line of the keratin-forming tumor cell line) were obtained from the cell bank of Shanghai Science Academy. Dulbecco's modified eagle medium (DMEM), fetal bovine serum, 0.25% trypsin-EDTA (1×), phosphate-buffered Saline (PBS), penicillin and streptomycin were obtained from Gibco. WST-1 (a Cell Proliferation and Cytotoxicity Assay Kit) was obtained from Beyotime.

3.2. Synthesis of AuNRs

AuNRs were synthesized according to the silver mediated method published.[26–31] It can be separated into two steps. Firstly, the synthesis of gold nanoseeds: $HAuCl_4$ (20 mM, 125 μL) and CTAB (0.1 M, 7.5 mL) were added into a 10 mL glass bottle with gentle mixing before a freshly prepared and ice-bathed $NaBH_4$ solution (10 mM, 0.6 mL) was injected, then the mixture was magnetically stirred until the color changed from golden yellow to brown which meant that 3.5 nm gold nanoseeds were obtained. The seed solution was then kept at 27 °C for at least 2 hours before usage. Secondly, the growth of gold nanorods: $HAuCl_4$ (20 mM, 250 μL) and $AgNO_3$ (10 mM, 100 μL) were added into CTAB (0.1 M, 10 mL) in a 20 mL glass bottle, followed by the addition of L-ascorbic acid (0.1 M, 60 μL) and the 10 time diluted gold seeds (120 μL). The growth solution was left at 27 °C overnight. Finally, CTAB stabilized AuNRs were prepared.

3.3. Coating AuNRs with mesoporous silica shell

Silica-coated gold nanorods were produced from CTAB-stabilized gold nanorods by utilizing the surface CTAB on AuNRs as a silane coupling agent for mesoporous silica coating. Through the process of hydration and condensation of TEOS, a silica layer can be formed on the surface of AuNRs according to the established method.[32–34] The sample solution was centrifuged twice to remove superfluous CTAB and then re-dispersed into 30 mL of deionized (D.I.) water, because excess CTAB may prevent the deposition of a uniform silica shell onto the AuNRs.[35] When the pH value of this solution was adjusted to about 10 with an NaOH solution under stirring, 10 μL of tetraethyl orthosilicate (TEOS) together with 10 μL of APTES was subsequently injected slowly under vigorous stirring for 30 min and then this course was repeated twice. The reaction mixture was allowed to proceed for a few hours to form an approximately 11 nm thick silica layer on the surface of AuNRs. Finally the AuNR@SiO_2 nanoparticles were isolated by centrifugation and washed with D.I. water several times, and then re-dissolved in D.I. water for further use. In the reaction course, the surface CTAB on the AuNRs works as a mould to form a mesoporous structure, enlarging the surface for more molecules to be adsorbed. The APTES provides amidogen on the silica shell, rendering the surface positively charged. Such a positively charged shell can improve the colloidal and shape stability of the nanorods.

3.4. Synthesis of mesoporous silica nanoparticles

Mesoporous silica nanoparticles (MSNs) were synthesized according to the method reported.[36–42] 0.2 g CTAB was dissolved in 100 mL of D.I. water before 0.6 mL of 2 M NaOH solution was added. The mixture was heated to 70 °C in an oil heating bath under vigorous magnetic stirring for 10 min. Then 1 mL of TEOS together with 100 μL APTES was added and mixed for a few minutes. 1 mL of EtoAc was continuously added and left for another 30 s. The solution was left undisturbed for more than 2 h. Then MSNs were obtained after centrifugation and washed with ethanol 3 times. Since amidogen was contained in mesoporous silica structures, these MSNs were also positively charged.

3.5. The preparation of composites

The molecular structure of Ce6 as is shown in Fig. 1E, shows the existence of a carboxyl group. Each Ce6 molecule possesses 3 negative electron charges, under the condition of complete ionization. Therefore, the composites of Ce6 with the above nanoparticles are easy to form due to the strong electrostatic attraction between the positively charged nanoparticles and the negatively charged Ce6 molecules. The composites of AuNR–Ce6, AuNR@SiO_2–Ce6 and MSN–Ce6 were prepared by mixing 1 mL 20 pM AuNR, AuNR@SiO_2 or MSN with 5 μL 1 mM Ce6 in dark and then shaking using a vortex overnight. Then the mixture was centrifuged to remove the un-conjugated Ce6 and re-suspended in an aqueous solution for subsequent usage.

3.6. Characterization of nanoparticles

Using an Agilent 8453 UV-visible/NIR spectrophotometer with quartz cuvettes of 10 mm optical path length, the absorption spectra of Ce6 and composite aqueous solutions were measured. The TEM images were taken by placing samples on carbon coated copper grids with a JEM-2100 transmission electron microscope operating at an accelerating voltage of 200 kV. Zeta potential was measured using the Malvern Zetasizer Nano S90 with a standard 633 nm laser.

3.7. Fluorescence measurements in solution

The fluorescence spectra were measured using a spectrometer (Hitachi, F-2500) with a 10 mm optical path quartz cuvette. The fluorescence lifetime was measured with the method of time-correlated single photon counting (TCSPC), which is based on the detection of single photons of a periodical light signal. A 2×10^7 Hz 405 nm Pico-second (ps) laser (Edinburgh Instruments, EPL405) was used for excitation. The fluorescence decay courses were measured by a PMT (Hamamatsu, R928P) with a band-pass filter of 665 ± 15 nm in the TCSPC (Edinburgh Instruments, TCC900). The obtained decay curves can be fitted with multi-exponential decay as described in formula (4), due to the fact that plasma intensity, which affects the radiation relaxation, depends on the relative position with respect to the AuNRs.[20,43]

$$I(t) = \sum_{i=1}^{n} \alpha_i \exp\left(-\frac{t}{\tau_i}\right) \tag{4}$$

where τ_i and α_i represent the decay constant and amplitude of each exponential component, respectively. The average lifetime $\bar{\tau}$ can be obtained according to formula (5)[25]

$$\bar{\tau} = \frac{\sum_{i=1}^{n} \alpha_i {\tau_i}^2}{\sum_{i=1}^{n} \alpha_i \tau_i} \tag{5}$$

The average fluorescence lifetimes of Ce6 in different cases were determined using the numerous measurements.

3.8. Cell culture

Cells were maintained in a DMEM medium with 10% calf serum, 100 units mL^{-1} penicillin, 100 μg mL^{-1} streptomycin and 100 μg mL^{-1} neomycin in a humidified standard incubator with a 5% CO_2 atmosphere at 37 °C. When the cells reached 80% confluence with normal morphology, the tested compound was added and the cells were incubated in the incubator for 3 hours for the case of the conjugates of AuNR@SiO_2–Ce6 or MSN–Ce6 and 5 hours for free Ce6. After that, these cells were washed three times with PBS. Then the cell samples were ready for fluorescence imaging measurements and fluorescence lifetime imaging measurements.

3.9. Fluorescence intensity imaging and fluorescence lifetime imaging

The fluorescence imaging of Ce6 in cells was acquired using a laser scanning confocal microscope (Olympus FV300, IX 71) equipped with a matched pinhole and a band-pass filter of 660 ± 15 nm in the detection channel. A water immersion objective (UplanApo, 60×, and 1.2 NA) was used in these measurements. A 405 nm continuous wave (CW) laser was used for common imaging excitation. Differential interference contrast (DIC) images were recorded simultaneously in a transmission channel to exhibit cell morphology.

The FLIM images of these composite loaded cells were acquired in parallel. The FLIM (Becker & Hickl GmbH, BDL-405-SMC ps laser, PMC-100 detector under the control of SPC-150 board and DCC-100) system was installed on the top cap of Olympus FV300 by replacing the dichroscope with a reflector. Under XY repeat model, the fluorescence photons from Ce6 excited by a 405 nm ps laser at a repetition rate of 20 MHz passed through a 660 ± 15 nm band-pass filter in the confocal fluorescence microscopy system to be collected by a photon counter (PMC-100). Then the lifetime of each pixel was figured out by fitting the intensity decay with the following exponential decay function:

$$I(t) = I_0 + A_1 \exp\left(-\frac{t}{\tau_1}\right) + A_2 \exp\left(-\frac{t}{\tau_2}\right) \tag{6}$$

Then according to formula (5) the intensity-weighted average lifetime (τ) of every pixel was calculated standing for the lifetime of the corresponding pixel. After XY repeat scanning of the 405 nm ps laser, the FLIM image was established.

3.10. Cytotoxicity of Ce6, and Ce6 composites

WST-1 was used to measure the dark toxicity of Ce6, AuNRs, MSNs and Ce6 composites on cells. A 200 μL cell suspension with a consistency of 10^3 cells per mL was seeded in each well of a 96-well flat bottom tissue culture plate and allowed to get attached to the plate and proliferate. When the cells reached 80% confluence with normal morphology, the Ce6 (5 μM), AuNR–Ce6 (20 pM–5 μM), AuNR@SiO_2–Ce6 (20 pM–5 μM) or MSN–Ce6 (20 pM–5 μM) composites were added into the corresponding wells, and incubated for a desired time. Then, the cells were incubated in 100 μL DMEM with 10 μL MTT solution (5 mg mL^{-1}) for another 2 h. Finally, the optical densities (O.D.) at 450 nm of each well were measured using an iEMS Analyzer (Lab-system). The cell viability in each well was determined by comparing the O.D. value with that of the untreated control cells in other wells of the same plate. All results were presented as mean ± SE from three independent experiments with 6 wells in each.

3.11. Singlet oxygen ($^1O_2$) measurements

DPBF, a sensitive $^1O_2$ probe, was used to measure the $^1O_2$ photo-produced by Ce6 in different situations. Upon oxidative degradation by $^1O_2$, the fluorescence of DBPF was quenched, so that the reducing rate of DPBF fluorescence in the sample solution was proportional to $^1O_2$ production. In the experiment DBPF (10 mM) was added into the sample solution. A 10 mW 660 ± 15 nm light was used to irradiate the sample solutions at 20 s intervals. Then the fluorescence of DBPF was measured accordingly to quantify the relative $^1O_2$ production.

3.12. PDT effect of Ce6 released from AuNR@SiO_2–Ce6 on cells

A culture plate with 96 wells, previously seeded in each well with 200 μL cells with a concentration of 3×10^3 cells mL^{-1}, was used in this experiment. When the cells reached 80% confluence with a normal morphology, AuNR@SiO_2–Ce6 (20 pM–5 μM) was added into each well and incubated for 3 h. After incubation, the cells were washed with PBS three times and replenished with a fresh medium. Then these cell wells were irradiated by a 780 nm laser (OEWindw MOGlabs) with a power density of 250 mW cm^{-2} for the desired number of times for different wells to measure the Ce6 released from cellular AuNR@SiO_2–Ce6 composites. After that, the cell wells were further irradiated by a CW light beam (660 ± 15 nm) with a power density of 10 mW cm^{-2} to carry out the Ce6 mediated PDT. After irradiation, the cells were incubated for another 24 h. Then, the cells were incubated in 100 μL DMEM with 10 μL MTT solution (5 mg mL^{-1}) for 2 h. Finally, the O.D. at 450 nm of each well was measured using an iEMS Analyzer (Lab-system). The cell viability in each well was determined by comparing the O.D. value with that of the untreated control cells in some wells of the same plate. All results were presented as mean ± SE from three independent experiments with 6 wells in each.

4. Conclusions

The mesoporous silica shell of AuNR@SiO_2 contained amidogen so that Ce6 molecules were easily conjugated on AuNRs to form AuNR@SiO_2–Ce6 with a loading efficiency of 80%. Due to the strong absorption of AuNRs at the LSPR band, a 780 nm laser can heat AuNR@SiO_2–Ce6 to release Ce6 making AuNR@SiO_2–Ce6 a photo-controllable Ce6 releasing composite. The fluorescence lifetime of conjugated Ce6 in AuNR@SiO_2–Ce6 was remarkably shortened to 0.9 ns in contrast to that of 6 ns when released. Utilizing the fluorescence lifetime difference between the conjugated Ce6 and free Ce6, we developed an FLIM technique to measure the photo-controllable Ce6 release from AuNR@SiO_2–Ce6 in living cells with a 780 nm laser. We found that a 780 nm laser beam can not only control the releasing amount of Ce6 from cellular AuNR@SiO_2–Ce6 by adjusting the irradiation dose of 780 nm laser but also precisely control the micro-region of Ce6 release in the cell by focusing the laser beam on the selected site. The free Ce6 is an efficient photosensitizer, whereas the PDT activity of AuNR@SiO_2–Ce6 is low because the $^1O_2$ generation ability of AuNR@SiO_2–Ce6 is remarkably limited. Therefore, controlling the Ce6 release of AuNR@SiO_2–Ce6 with a 780 nm laser can control the PDT effect of AuNR@SiO_2–Ce6, which is confirmed in PDT killing experiments on both KB and Hela cells. We believe that the controllable PDT effect has great potentials in PDT practices as it releases photosensitizers on tumour sites only thus preventing skin photo-toxicity.

Acknowledgements

Financial support from the National Natural Science Foundation of China (11074053 and 31170802) is gratefully acknowledged.

Notes and references

1 D. Pissuwan, T. Niidome and M. B. Cortie, *J. Controlled Release*, 2011, **149**, 65–71.
2 J. L. Vivero-Escoto, I. I. Slowing, C. W. Wu and V. S. Y. Lin, *J. Am. Chem. Soc.*, 2009, **131**, 3462–3463.
3 Y. N. Zhao, B. G. Trewyn, I. I. Slowing and V. S. Y. Lin, *J. Am. Chem. Soc.*, 2009, **131**, 8398–8400.
4 K. K. Coti, M. E. Belowich, M. Liong, M. W. Ambrogio, Y. A. Lau, H. A. Khatib, J. I. Zink, N. M. Khashab and J. F. Stoddart, *Nanoscale*, 2009, **1**, 16–39.
5 Z. J. Zhang, L. M. Wang, J. Wang, X. M. Jiang, X. H. Li, Z. J. Hu, Y. H. Ji, X. C. Wu and C. Y. Chen, *Adv. Mater.*, 2012, **24**, 1418–1423.

6 T. Luo, P. Huang, G. Gao, G. X. Shen, S. Fu, D. X. Cui, C. Q. Zhou and Q. S. Ren, *Opt. Express*, 2011, **19**, 17030–17039.
7 C. D. S. Brites, P. P. Lima, N. J. O. Silva, A. Millan, V. S. Amaral, F. Palacio and L. D. Carlos, *Nanoscale*, 2012, **4**, 4799–4829.
8 J. A. Webb and R. Bardhan, *Nanoscale*, 2014, **6**, 2502–2530.
9 C. Y. Li and J. F. Zhu, *Mater. Lett.*, 2013, **112**, 169–172.
10 J. Malicka, I. Gryczynski and J. R. Lakowicz, *Biochem. Biophys. Res. Commun.*, 2003, **306**, 213–218.
11 J. Chen, Y. H. Jin, N. Fahruddin and J. X. Zhao, *Langmuir*, 2013, **29**, 1584–1591.
12 X. Li, F. J. Kao, C. C. Chuang and S. L. He, *Opt. Express*, 2010, **18**, 11335–11346.
13 X. H. Huang, P. K. Jain, I. H. El-Sayed and M. A. El-Sayed, *Lasers Med. Sci.*, 2008, **23**, 217–228.
14 E. B. Dickerson, E. C. Dreaden, X. H. Huang, I. H. El-Sayed, H. H. Chu, S. Pushpanketh, J. F. McDonald and M. A. El-Sayed, *Cancer Lett.*, 2008, **269**, 57–66.
15 Y. K. Xu, S. Kim and J. Y. Chen, *ACS Appl. Mater. Interfaces*, 2014, **6**(10), 5619–5628.
16 X. Wu, J. Y. Chen, A. Brech, C. H. Fang, J. F. Wang, P. J. Helm and Q. Peng, *Biomaterials*, 2013, **34**, 6157–6162.
17 G. M. Santos, F. S. Zhao, J. B. Zeng and W. C. Shih, *Nanoscale*, 2014, **6**, 5718–5724.
18 Z. Zhang, J. Wang, X. Nie, T. Wen, Y. Ji, X. Wu, Y. Zhao and C. Chen, *J. Am. Chem. Soc.*, 2014, **136**, 7317–7326.
19 W. Li, X. Cai, C. Kim, G. Sun, Y. Zhang, R. Deng, M. Yang, J. Chen, S. Achilefu, L. V. Wang and Y. Xia, *Nanoscale*, 2011, **3**, 1724–1730.
20 N. S. Abadeer, M. R. Brennan, W. L. Wilson and C. J. Murphy, *ACS Nano*, 2014, **8**, 8392–8406.
21 B. Stella, S. Arpicco, M. T. Peracchia, D. Desmaele, J. Hoebeke, M. Renoir, J. D'Angelo, L. Cattel and P. Couvreur, *J. Pharm. Sci.*, 2000, **89**, 1452–1464.
22 W. C. Chen, A. X. Zhang and S.-D. Li, *Eur. J. Nanomed.*, 2012, **4**, 89–93.
23 K. Greish, *J. Drug Targeting*, 2007, **15**, 457–464.
24 A. Samanta, Y. D. Zhou, S. L. Zou, H. Yan and Y. Liu, *Nano Lett.*, 2014, **14**, 5052–5057.
25 R. Yasuda, C. D. Harvey, H. N. Zhong, A. Sobczyk, L. van Aelst and K. Svoboda, *Nat. Neurosci.*, 2006, **9**, 283–291.
26 S. Eustis and M. El-Sayed, *J. Phys. Chem. B*, 2005, **109**, 16350–16356.
27 M. A. Mahmoud and M. A. El-Sayed, *J. Phys. Chem. Lett.*, 2013, **4**, 1541–1545.
28 M. B. Mohamed, V. Volkov, S. Link and M. A. El-Sayed, *Chem. Phys. Lett.*, 2000, **317**, 517–523.
29 W. Ni, X. Kou, Z. Yang and J. Wang, *ACS Nano*, 2008, **2**, 677–686.
30 T. K. Sau and C. J. Murphy, *J. Am. Chem. Soc.*, 2004, **126**, 8648–8649.
31 J. E. Park, M. Atobe and T. Fuchigami, *Ultrason. Sonochem.*, 2006, **13**, 237–241.
32 Y. S. Chen, W. Frey, S. Kim, P. Kruizinga, K. Homan and S. Emelianov, *Nano Lett.*, 2011, **11**, 348–354.
33 J. V. Jokerst, M. Thangaraj, P. J. Kempen, R. Sinclair and S. S. Gambhir, *ACS Nano*, 2012, **6**, 5920–5930.
34 X. J. Tian, J. Guo, Y. Tian, H. Y. Tang and W. L. Yang, *RSC Adv.*, 2014, **4**, 9343–9348.
35 Y. Lu, Y. D. Yin, Z. Y. Li and Y. N. Xia, *Nano Lett.*, 2002, **2**, 785–788.
36 J. Kim, H. S. Kim, N. Lee, T. Kim, H. Kim, T. Yu, I. C. Song, W. K. Moon and T. Hyeon, *Angew. Chem., Int. Ed.*, 2008, **47**, 8438–8441.
37 J. Lu, M. Liong, J. I. Zink and F. Tamanoi, *Small*, 2007, **3**, 1341–1346.
38 I. I. Slowing, B. G. Trewyn, S. Giri and V. S. Y. Lin, *Adv. Funct. Mater.*, 2007, **17**, 1225–1236.
39 I. I. Slowing, B. G. Trewyn and V. S. Y. Lin, *J. Am. Chem. Soc.*, 2007, **129**, 8845–8849.
40 I. I. Slowing, J. L. Vivero-Escoto, C. W. Wu and V. S. Y. Lin, *Adv. Drug Delivery Rev.*, 2008, **60**, 1278–1288.
41 F. Torney, B. G. Trewyn, V. S. Y. Lin and K. Wang, *Nat. Nanotechnol.*, 2007, **2**, 295–300.
42 J. L. Vivero-Escoto, I. I. Slowing, B. G. Trewyn and V. S. Y. Lin, *Small*, 2010, **6**, 1952–1967.
43 S. Khatua, P. M. R. Paulo, H. F. Yuan, A. Gupta, P. Zijlstra and M. Orrit, *ACS Nano*, 2014, **8**, 4440–4449.

